Received: 25 September 2017 | Revised: 4 August 2018 | Accepted: 8 August 2018

DOI: 10.1002/joc.5839

International Journal of Climatology RMetS

RESEARCH ARTICLE

Evaluation of TMPA 3B42V7, GPM IMERG and CMPA precipitation estimates in Guangdong Province, China

Dashan Wang[1] | Xianwei Wang[1] | Lin Liu[2,3] | Dagang Wang[1] | Huabing Huang[1] | Cuilin Pan[1]

[1]Guangdong Key Laboratory for Urbanization and Geo-simulation, Center of Integrated Geographic Information Analysis, School of Geography and Planning, Sun Yat-sen University, Guangzhou, China

[2]Department of Geography, University of Cincinnati, Cincinnati, Ohio

[3]School of Geographical Sciences, Center of GeoInformatics for Public Security, Guangzhou University, Guangzhou, China

Correspondence
Xianwei Wang, Guangdong Key Laboratory for Urbanization and Geo-simulation, Center of Integrated Geographic Information Analysis, School of Geography and Planning, Sun Yat-sen University, Guangzhou, China.
Email: wangxw8@mail.sysu.edu.cn
Lin Liu, Department of Geography, University of Cincinnati, Cincinnati, OH.
Email: lin.liu@uc.edu

Funding information
Guangdong Research Station of Science and Technology Experts, Grant/Award Number: 2015A090905002; National Natural Science Foundation of China, Grant/Award Number: #51779278; Science and Technology Program of Guangzhou, Grant/Award Number: #1561000154, #201707010098; Water Resource Science and Technology Innovation Program of Guangdong Province, Grant/Award Number: #2016-19

Three satellite rainfall products (3B42V7, IMERGV05/V04/V03, and China hourly Merged Precipitation Analysis product) are evaluated using measurements from a dense rain gauge network as reference in Guangdong Province, China from April 2014 to December 2016. The three products are compared with gauges in annual, monthly, daily and hourly accumulation, and at gridded, sub-regional and regional scales. An error decomposition approach is employed to separate the total bias into Hit, Miss and False components. Overall, the CMPA estimate is the best in agreement with gauge observations. The improvement of IMERGV05 over 3B42V7 is notable, especially in reducing the hit bias and missed precipitation, resulting in better detection of the light rain and heavy rain. The enhancement of IMERG is more significant at the 3-hr scale than daily scale. IMERGV05 shows better performance than its previous versions especially for IMERGV03, which had an abnormal blocky pattern mainly from July to September over the Pearl River Delta area. The three products have different error characteristics and show large spatial variations. 3B42V7 and IMERG have large areas of overestimation in the mountainous areas and underestimation in the coastal areas, while CMPA is characterized by an alternate distribution of small positive and negative values. The overestimation of precipitation is partially attributed to the positive hit biases that falsely estimate the precipitation from moderate intensity to heavy rainfall by the three products.

KEYWORDS
CMPA, evaluation, GPM IMERGV05, precipitation, TMPA 3B42V7

1 | INTRODUCTION

Satellite-based precipitation products have been rapidly developed and widely used for their high resolution, easy access and global coverage. Most satellite-based precipitation products merge data from passive microwave (PMW) sensors with those from low-earth-orbiting (LEO) (Ferraro, 1997) and geostationary satellite infrared (IR) sensors (Xie and Arkin, 1998). Rain gauge observations such as the Global Precipitation Climatology Center (GPCC) monthly precipitation analysis (Schneider *et al.,* 2011) are also merged in some precipitation estimates to reduce the bias (Xie and Xiong, 2011).

Many satellite precipitation products have become available to the public during the past decades, such as the Tropical Rainfall Measurement Mission (TRMM) (Huffman *et al.,* 2007), the Precipitation Estimation from Remotely Sensed Information using Artificial Neural Network (PERSIANN) (Sorooshian *et al.,* 2000), the Global Satellite Mapping of Precipitation (GSMaP) (Kubota *et al.,* 2007), the Climate Prediction Center Morphing Technique (CMORPH) (Joyce *et al.,* 2004), and the China hourly Merged Precipitation Analysis product (CMPA) (Shen *et al.,* 2014). The TRMM Multi-Satellite Precipitation Analysis (TMPA) is intended to produce the "best" quasi-global (50°N–50°S) precipitation estimate (Huffman *et al.,* 2007;

Yong *et al.,* 2015). The latest TMPA (Version 7) has been available since January 2013. Several studies have demonstrated the improvement of data quality from V6 to V7 (Chen *et al.,* 2013a; Chen *et al.,* 2013b; Melo *et al.,* 2015; Prakash *et al.,* 2015). As an extension of the TRMM satellite, the Global Precipitation Measurement (GPM) core observatory was launched on February 27, 2014, marking the transition from the TRMM-era to the GPM-era (Hou *et al.,* 2014). The GPM is expected to provide more reliable global precipitation products (90°N–90°S) than TMPA (Liu and Zipser, 2015). The Day-1 Integrated Multi-satellitE Retrievals for GPM (IMERG) (Huffman *et al.,* 2018) was released recently with 0.1° and half-hour resolution, which is finer than that of 0.25° and 3-hr of the TMPA products. These satellite-based precipitation products have been widely applied in hydrologic predictions (Su *et al.,* 2008; Yong *et al.,* 2010), numerical model validations (Ebert *et al.,* 2007), climate variability (Dai *et al.,* 2007; Zhou *et al.,* 2008) and flood and drought monitor (Hossain and Lettenmaier, 2006; Rhee *et al.,* 2010). They could bring remarkable benefits to the society, especially for developing countries and remote areas with sparse or poor-quality gauge networks and weather radars (Gao and Liu, 2013; Xue *et al.,* 2013).

Despite the great utility of satellite-based precipitation estimates, the data uncertainty is still large (Tian and Peters-Lidard, 2010). Satellite based precipitation estimates suffer from two major error sources: the sampling error, which arises from the discrete revisit time and the gaps in spatial cover, and the retrieval error, which results from the retrieval relationship between satellite observations and rain rates (Tang *et al.,* 2015). Compared to the former, the latter is more complex and may be affected by sensor parameters, cloud/precipitation type, topography, atmospheric condition and the retrieval model (Arkin and Xie, 1994; McCollum *et al.,* 2002; Tian and Peters-Lidard, 2007). Besides, the quality of input satellite data and ground gauge observations could also affect the accuracy of Satellite based precipitation estimates. Although the source sensors of some satellite-based precipitation products may be nearly the same, the retrieval methods merging and interpolating data could vary significantly from one product to another. Therefore, it is essential to assess the sources and characteristics of retrieval errors for gaining insight into accuracy and data uncertainty of these products. Doing so can help the data producers to improve the retrieval algorithm for enhancing the data quality (Kidd and Levizzani, 2011; Tang *et al.,* 2016), or the data users to select suitable products for their particular applications (Hossain and Huffman, 2008; Tian *et al.,* 2009).

The performance of different products varies with areas since the retrieval errors differ in different surface conditions, climate regions, and seasons (Sorooshian *et al.,* 2011). A substantial number of studies have compared the performance of different satellite-based precipitation estimates (e.g., Shen *et al.,* 2010; Stampoulis and Anagnostou, 2012; Chen *et al.,* 2013a; Chen *et al.,* 2013b; Mei *et al.,* 2014). Some efforts have been made to compare the performance TMPA and IMERG estimates at the early stage of GPM-era (e.g., Guo *et al.,* 2016; Prakash *et al.,* 2016; Sharifi *et al.,* 2016). Tang *et al*. (2016) compared the performance of IMERG Version 03 (IMERGV03) and 3B42V7 over mainland China, and found that IMERGV03 shows better performance at multiple timescales and over different regions. Xu *et al*. (2017) compared the IMERGV03 and 3B42V7 products in southern Tibetan Plateau region and confirmed the better performance of IMERGV03 in different elevation ranges.

IMERGV04 was released to replace the IMERGV03 in late March 2017, and the latest IMERGV05 was available since January 2018 (Huffman *et al.,* 2018). Although many evaluation works have been done in previous studies, the performance and improvement of the latest GPM IMERG estimate (IMERGV05) against its predecessor TMPA products and IMERGV04/03 over the tropical southern China, as well as the CMPA estimate, needs further investigations. The primary objectives of this study are: (1) to compare the 3B42V7, IMERGV05 and CMPA products against the ground gauge observations at 0.25° grids to explore their differences; (2) to compare the IMERGV05/04 and CMPA at 0.1° grids to demonstrate the improvement and limitation of IMERG; (3) to investigate the characteristics and variations of different error components in these three products.

2 | DATA AND METHODS

2.1 | Study area and climatology

Guangdong Province lies in the southern China from 109° to 118° E and from 20° to 26° N (Figure 1a). It is the downstream of the Pearl River and the north of the South China Sea. The topography in Guangdong is complex with mountainous areas in the northern and eastern parts and low land in the central and coastal parts. The tropical to subtropical monsoon climate prevails with a hot and wet summer. The wet season from April to September holds 80% of annual precipitation (~1,800 mm; Figure 1b,c). The annual mean air temperature is 22 °C (Wang *et al.,* 2016).

Guangdong Province consists of 21 prefecture-level cities and is adjacent to the special administrative regions of Hong Kong and Macao (Figure 1a). The 21 cities/regions are Guangzhou (GZ), Shenzhen (SZ), Zhuhai (ZH), Dongguan (DG), Foshan (FS), Zhongshan (ZS), Jiangmen (JM), Zhaoqing (ZQ), Huizhou (HZ), Shantou (ST), Chaozhou (CZ), Jieyang (JY), Shanwei (SW), Zhanjiang (ZJ), Maoming (MM), Yangjiang (YJ), Shaoguan (SG), Qingyuan (QY), Yunfu (YF), Meizhou (MZ), and Heyuan (HY). Guangdong, especially the Pearl River Delta (PRD) region, is of great importance to the socio-economic development of China.

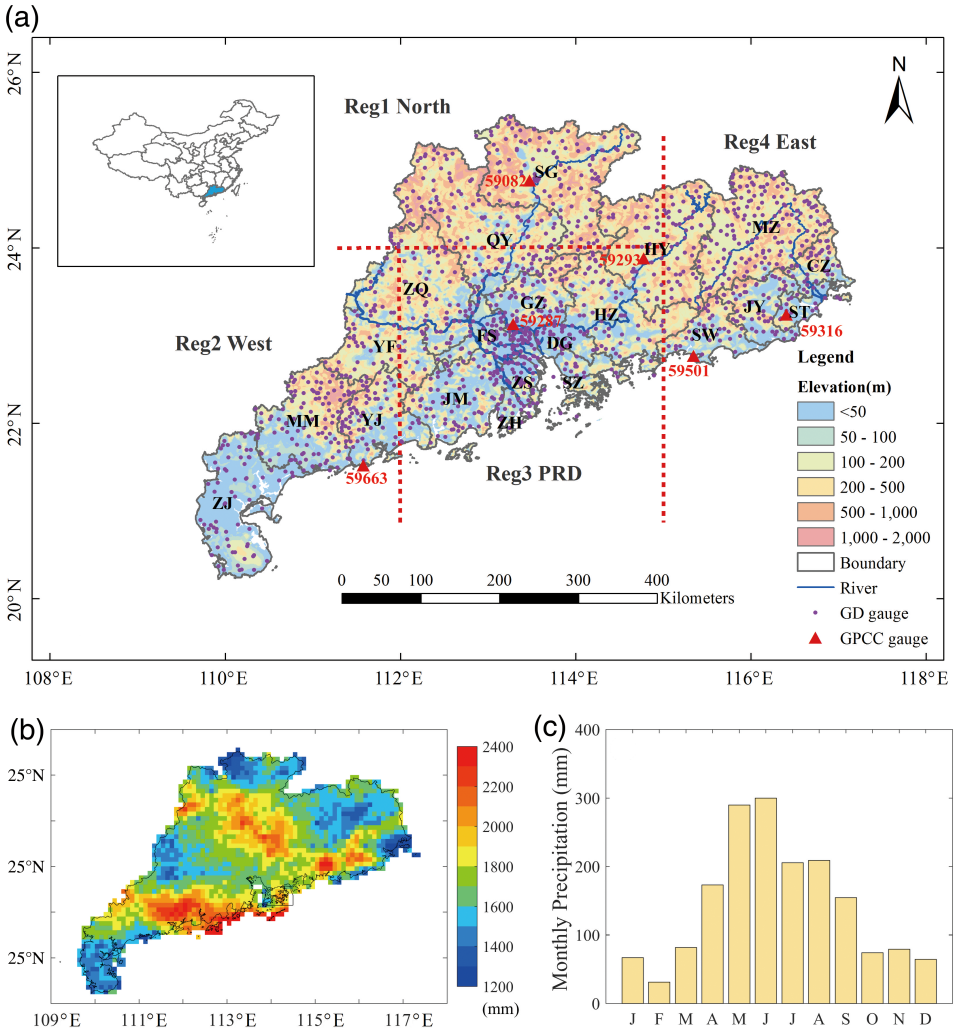

FIGURE 1 (a) Topography, major rivers, dense rain gauges (dots), and six International Exchange Stations involved in GPCC (triangles) in Guangdong Province, China. The 21 prefecture-level cities are marked with 2 capital letters. The dash lines outline the four sub-regions in this study: Reg1: the northern mountainous area; Reg2: the western coastal area; Reg3: the central Pearl River Delta (RPD); and Reg4: the eastern coastal and mountainous areas of Guangdong Province. (b) Spatial distribution of annual mean precipitation in Guangdong Province. (c) Monthly spatial mean precipitation over Guangdong Province. Precipitation data are derived from CMPA estimate ranging from 2008 to 2016 [Colour figure can be viewed at wileyonlinelibrary.com]

The permanent residents of Guangdong Province exceeded 107 million in 2014, and the Gross Domestic Product (GDP) reached 6,780 billion Yuan, accounting for more than 1/6 of the nation's total GDP (Wang and Zhu, 2016). As the population grows and economics blooms, the frequent occurring flooding inside the cities and over mountainous areas caused by heavy precipitation have become a severe threat to residents, agriculture, industry, and social economy.

2.2 | Satellite precipitation products

The latest Version-7 post-real-time research-grade product of TMPA 3B42 (hereafter 3B42V7) at the 3-hr and 0.25° resolution was used in this study (TRMM Science Team, 2013; ftp://arthurhou.pps.eosdis.nasa.gov/trmmdata/). 3B42V7 integrates three types of observations such as the Precipitation Radar (PR), PMW and IR from several satellite-borne sensors. All PMW estimates are first calculated using the Goddard profiling algorithm and then calibrated and combined by considering TRMM's Microwave Imager (TMI) estimates as reference. The available IR estimates are produced based on the calibrated PMW estimates. At last the PMW and IR estimates are combined, and a bias correction is carried out using the GPCC monthly gauge analysis to enhance the calibration (Huffman *et al.*, 2007). The latest 3B42V7 has remarkable improvements compared to the earlier versions, including additional satellite inputs, high quality surface gauge data, uniformed retrieval algorithms and reflectivity-rain-rate relationship, and a latitude band calibration system (Huffman *et al.*, 2018). Chen *et al.* (2013a, 2013b) found that 3B42-V7 successfully improves the agreement with observations and reduces the data bias over most regions in continental US and mainland China.

The GPM, which includes the GPM Core Observatory and 10 partner satellites, is a constellation-based satellite mission designed to provide a new generation of precipitation estimates (Hou *et al.*, 2014). The GPM core satellite

carries a dual-frequency precipitation radar (DPR) and a conical-scanning multichannel GPM Microwave Imager (GMI), which largely extends the sensor packages and expands the frequency of sensors (Table 1). In addition, GPM has increased the orbital inclination to 65° from 35° of TRMM, to afford wider coverage of important climate zones (Huffman *et al.,* 2018). These upgraded sensors are used together with other sensors on the constellation satellites to develop the new Day-1 Integrated Multi-satellitE calibration algorithm for GPM (IMERG). The latest Version-05 algorithms were developed in May 2017. IMERG provides three products: the early run and the late run, which are the two near-real-time products and have a latency of 4 and 12 hr, respectively, and the final run, which is a post real-time product with a latency of 4 months. The latest IMERG V05 final run product (hereafter IMERGV05) is analysed in this study (GPM Science Team, 2018; ftp://arthurhou.pps.eosdis.nasa.gov/gpmdata/), and the IMERGV04/V03 are also illustrated for comparison against IMERGV05. IMERGV05 fixes some evident problems (e.g., spatial blocky pattern) of IMERGV03 and integrate the strengths from three previous multi-satellite precipitation products including the TMPA from NASA (Huffman *et al.,* 2007), the CMORPH from NOAA (Joyce *et al.,* 2004), and the PERSIANN from University of California Irvine (Sorooshian *et al.,* 2000). With these strengths, it is expected to bring new insights to light and heavy rain, solid precipitation, storm structures and precipitation microphysics (Hou *et al.,* 2014).

The CMPA (Shen *et al.,* 2014; data source: http://data.cma.cn/data/online.html?t=6) is derived from merging the 8 km/30 min CMORPH data with a dense rain gauge network from the China Meteorology Administration (CMA). At first, the hourly precipitation measurements from near 30,000 automatic weather stations over China are interpolated into 0.1°× 0.1° grids. Then the raw CMORPH estimates are resampled and summed into 0.1°× 0.1° grids and hourly accumulation. The resampled CMORPH data are calibrated based on probability density function (PDF) technique and merged with the gauge data using an improved optimum interpolation technique (Shen *et al.,* 2014). The final CMPA estimate covers a period from January 2008 to present. This merged precipitation estimate combines the advantages from both the raw satellite-based data and the gauge observations over mainland China (Chen *et al.,* 2016a).

The details of the three precipitation products are given in Table 1. The evaluation period is from April 2014 to the end of 2016. The three products are aggregated from the original scale to daily, 3-hr and hourly (only for IMERG and CMPA) accumulation for analysis. Since the spatial resolutions of the three estimates are different, it may cause scaling effects that the satellite precipitation datasets with coarse grids tend to present better accuracy than those with finer grids if we conduct the analysis at their origin spatial resolutions. We upscaled the IMERG and CMPA products into 0.25°× 0.25° grids to match 3B42V7 using the standard bilinear interpolation method as Guo *et al*. (2016) suggested.

2.3 | Ground reference

Hourly precipitation data from a dense rain gauge network is provided by the Department of Water Resources in Guangdong Province (data source: http://www.gdwater.gov.cn/). All precipitation data are hourly recorded with a precision of 0.1 mm. The ground observation network includes more than 1,800 automatic rain gauges, and the rainfall data are available since October 2012. All the gauge rainfall data from April 2014 to December 2016 are screened by a strict quality control approach (Ren *et al.,* 2010). This approach includes three quality checks: the extreme values check, the internal consistency check and the spatial consistency check. There are 1,416 gauges with valid precipitation observation after quality control. These gauge observations were further checked by comparing the six International Exchange Stations that involved in GPCC data (Figure 1a). However, these automatic rain gauges had systematical biases during the last 15 days in April of 2015 and the first 5 days in August of 2016, which were excluded in the following evaluation study. The gauges are densely distributed even in the mountainous area. To the best of our knowledge, these gauges are not involved in the interpolation process of 3B42V7, IMERG, or CMPA estimates. The gauge observations were used to evaluate the CMPA estimates in terms of

TABLE 1 Basic information of the 3B42V7, IMERG and CMPA estimates

Products	3B42V7	IMERG	CMPA
Data sources	TMI, SSM/I, SSMIS, AMSU-B, AMSR-E, MHS, Geo-IR, TCI, monthly gauge observations	AMSR2, SSM/I, SSMIS, AMSU-B, MHS, SAPHIR, GMI, ATMS, Geo-IR, AIRS, TOVS, CRIS, TCI, monthly gauge observations	CMORPH (TMI, AMSR-E, AMSR2, SSM/I, SSMIS, AMSU-B, MHS, Geo-IR) and hourly gauge observations
Precipitation radar	PR; Ku-band at 13.8 GHz	DPR; Ku-band at 13.6 GHz and Ka-band at 35.5 GHz	CMORPH (PR)
Microwave imager	TMI; frequencies range between 10 and 85.5 GHz	GMI; frequencies range between 10 and 183 GHz	CMORPH (TMI)
Coverage	50°S–50°N	90°S–90°N	70°–140°E, 15°–59°N
Resolution	0.25°× 0.25°and 3-hr	0.1°× 0.1°and half-hour	0.1°× 0.1°and hour
Availability	January 1998 to date	mid-March 2014 to date	January 2008 to date

Note. References Hou *et al.,* (2014), Shen *et al.,* (2014), Yong *et al.,* (2015), Huffman *et al.,* (2018).

typhoon related rainfall events during 2013 to 2015 (Wang *et al.,* 2016).

2.4 | Methodology

To evaluate the three satellite-based precipitation estimates, several metrics are selected, including four traditional metrics and three error decomposition components. The equations and units of these metrics are given in Table 2. Correlation coefficient (CC) could describe the linear variation agreement between the satellite estimates and gauge-based reference. Relative bias (RB) and Bias could indicate the accumulative retrieval bias of estimates, and root mean square difference (RMSD) could show the average magnitude of error. CC and RB are dimensionless, while RMSD and Bias are in mm, mm/day or mm/hr, depending on the temporal scale of analysis. These four metrics are used together to compare satellite-based precipitation products with gauge observations in this study, and they are also widely used in other validation studies (Yong *et al.,* 2010; Jiang *et al.,* 2012; Guo *et al.,* 2016).

For each product, the total bias of daily precipitation over Guangdong Province are further decomposed into the three error components at the grid scale following by the method of Tian *et al*. (2009), namely the hit bias, the missed precipitation, and the false precipitation. The Hit (H), Miss (−M) and False (F) parts are separated based on a contingency table (see Ebert *et al.,* 2007 for detail). The total bias (E) and its three error components have the relationship as: E = H-M + F. Three categorical statistics can be determined based on the count of Hit, Miss and False components (Table 2). Probability of detection (POD) responds to the fraction of the gauge observed rain hours that are correctly detected by the satellite products. False alarm ratio (FAR) represents the ratio of precipitation that didn't occur among the satellite estimates. Critical success index (CSI) indicates the overall ratio of rain hours correctly captured by the satellite products.

The study area is further divided into four sub-regions to investigate the spatial variations of the three products (Figure 1a). The four sub-regions are originally determined according to the apparent blocky pattern of IMERGV03 estimate found in our preliminary analysis (also illustrated in Figure 5e–h). To investigate the temporal performance of the precipitation estimates in Guangdong and the four sub-regions, four seasons are divided as January-February-March (JFM), April-May-June (AMJ), July-August-September (JAS) and October-November-December (OND), to fit the climatology of Guangdong Province where the first rainy season happens during AMJ and the second rainy season happens during JAS. Diurnal variability is one of the most important temporal characteristics of precipitation and has been pronounced by many researches (Dai *et al.,* 2007; Zhou *et al.,* 2008; Chen *et al.,* 2016b). Since nearly 80% of the annual precipitation occurs during the rainy season over Guangdong Province, the diurnal cycle of IMERGV05, CMPA and Gauge observation over the four sub-regions are calculated during the first rainy season (April–June) and the second rainy season (July–September) separately using hourly precipitation data. Diurnal values are converted from UTC to the Local Solar Time (LST) of China. To reveal the performance of satellite estimate in capturing precipitation within different levels, the probability distribution functions (PDF) for satellite precipitation estimates and gauge observations are compared.

The rain/no-rain threshold is set to 0.1 mm/hr for the 3B42V7, IMERG, CMPA and gauge observations in calculating four traditional metrics and three error decomposition components. The common grid-to-point comparison method (Yong *et al.,* 2010; Li *et al.,* 2013) is adopted in this study, but only grids with at least one gauge are taken for

TABLE 2 Statistical metrics used in this study

Metrics	Equation	Unit	Perfect value
Correlation coefficient (CC)	$CC = \frac{\sum_{i=1}^{n}(G_i-\overline{G})(S_i-\overline{S})}{\sqrt{\sum_{i=1}^{n}(G_i-\overline{G})^2}\sqrt{\sum_{i=1}^{n}(S_i-\overline{S})^2}}$	/	1
Relative bias (RB)	$RB = \frac{\sum_{i=1}^{n}(S_i-G_i)}{\sum_{i=1}^{n}G_i} * 100\%$	%	0
Root mean square difference (RMSD)	$RMSD = \sqrt{\frac{1}{n}\sum_{i=1}^{n}(S_i-G_i)^2}$	mm	0
Total bias (bias)	$Bias = \sum_{i=1}^{n}S_i - \sum_{j=1}^{m}G_j$	mm	0
Hit bias	$Hit = \sum_{i=1}^{n}(S_i-G_i)$, when $S_i>0$ *and* $G_i>0$	mm	0
Missed precipitation	$Miss = \sum_{i=1}^{n}(S_i-G_i)$, when $S_i=0$ *and* $G_i>0$	mm	0
False precipitation	$False = \sum_{i=1}^{n}(S_i-G_i)$, when $S_i>0$ *and* $G_i=0$	mm	0
Probability of detection (POD)	$POD = \frac{N_{hit}}{N_{hit}+N_{miss}}$	/	1
False alarm ratio (FAR)	$FAR = \frac{N_{false}}{N_{hit}+N_{false}}$	/	0
Critical success index (CSI)	$CSI = \frac{N_{hit}}{N_{hit}+N_{miss}+N_{false}}$	/	1

Notes. i and j represent the spatial grid points; n and m are the total number of grid samples; G and S are the gauge observations and satellite estimates, respectively. Hit means precipitation observed by the satellite estimate and gauge simultaneously; Miss represents precipitation observed by the gauge while not detected by the satellite estimate; False is on the contrary of Miss, that is, precipitation detected by the satellite estimate while not observed by the gauge.

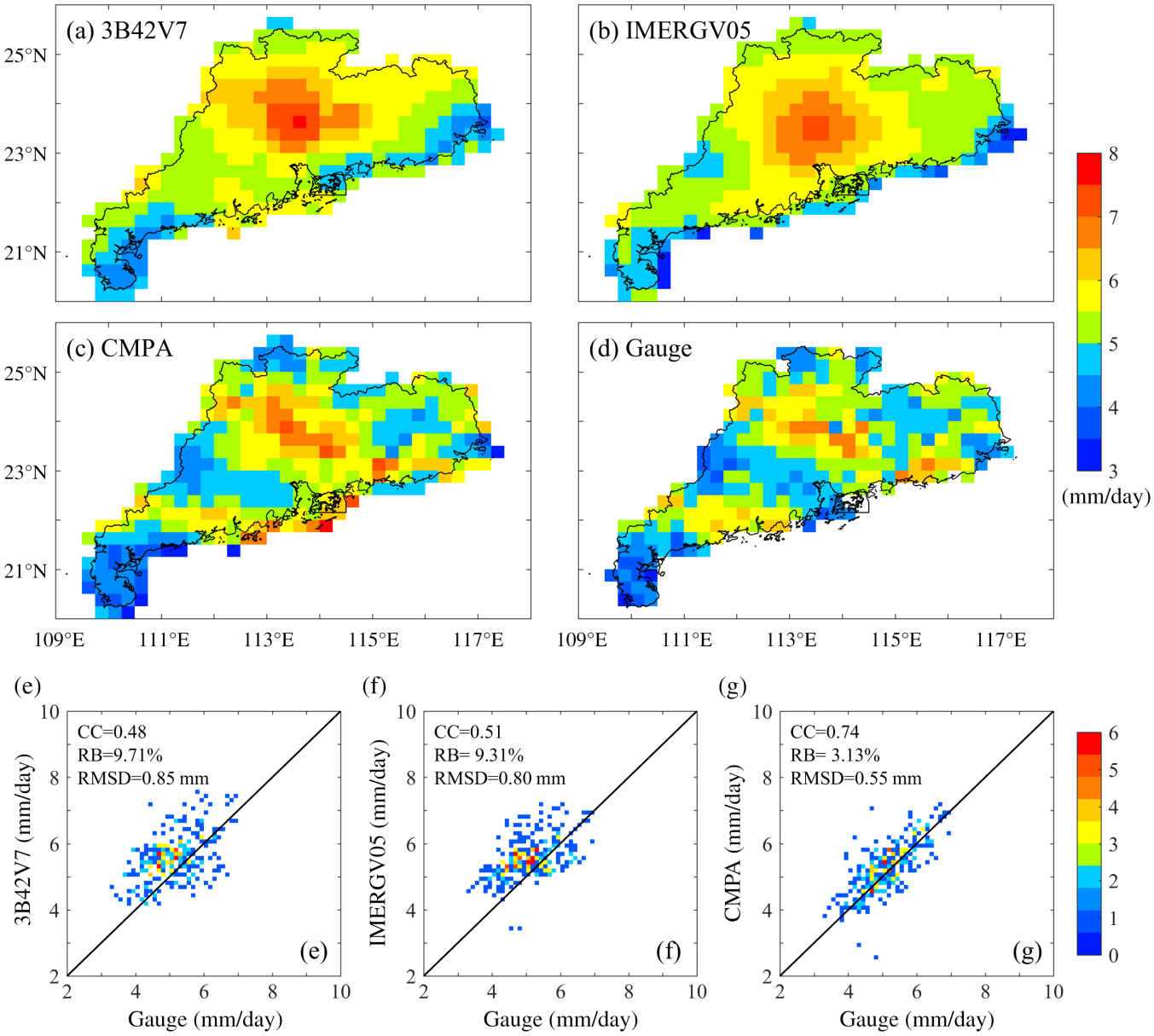

FIGURE 2 Spatial distribution of the daily mean precipitation ranging from April 2014 to December 2016 derived from (a) TMPA 3B42V7, (b) GPM IMERGV05, (c) CMPA, and (d) gauge observation in Guangdong Province, China, and the density-colour scatter plots of gauge data versus (e) TMPA 3B42V7, (f) GPM IMERGV05, and (g) CMPA. The density is the number of grids within a rain depth interval of 0.125 mm/day [Colour figure can be viewed at wileyonlinelibrary.com]

evaluation. The mean value of all gauge measurements within a single grid box is calculated if there are more than one gauge.

3 | RESULTS

3.1 | Comparison of 3B42V7 and IMERGV05 at 0.25° grid

There are three precipitation centres in Guangdong Province (Figure 1b), that is, the north of the Pearl River's Estuary, the western coastal area (mainly in MM and YJ), and the eastern coastal area (mainly in SW). The daily mean precipitation over the three centres is higher than 6 mm/day and is much higher than that over the northern and eastern mountainous area and the southwestern Leizhou Peninsula (Figure 2d). 3B42V7 and IMERGV05 generally exhibit a similar spatial pattern with gauges except for underestimation over the western and eastern coastal areas, and overestimation over the north of the Pearl River's Estuary (Figure 2). The error statistics reveal that all the three products overestimate the total precipitation with positive RBs (9.71, 9.31 and 3.13%, respectively). CMPA performs well in capturing the spatial pattern of precipitation over Guangdong Province. CMPA shows much better performance than 3B42V7 and IMERGV05 (Figure 2e–g), with much higher CC and lower RMSD/RB. It is reasonable because CMPA integrated hourly observations from numerous gauges.

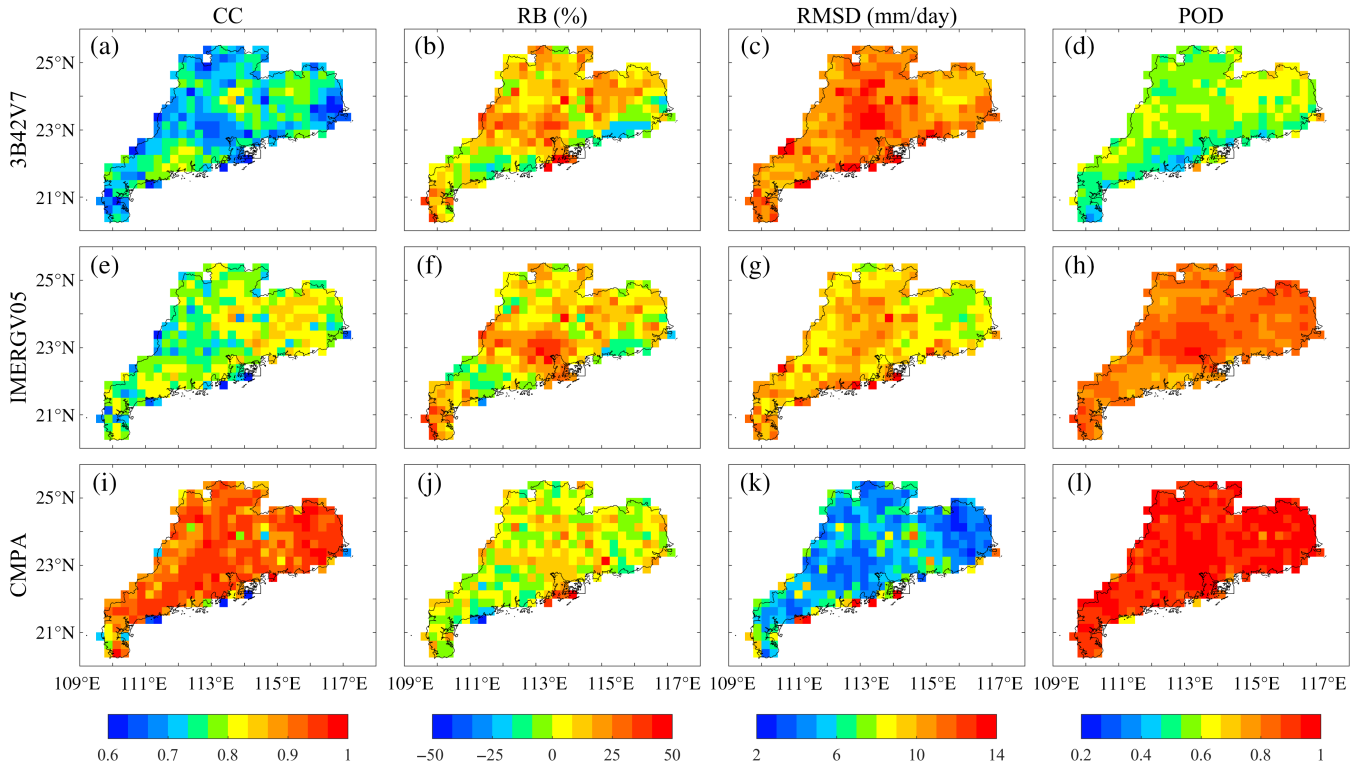

FIGURE 3 Spatial distribution of the correlation coefficient (a, e, i), relative bias (b, f, j), root mean square difference (c, g, k), and POD (d, h, l) for the 3B42V7, IMERGV05 and CMPA products against rain gauge observations in Guangdong Province, China. All metrics were computed using the daily precipitation series at each 0.25° grid ranging from April 2014 to December 2016 [Colour figure can be viewed at wileyonlinelibrary.com]

3B42V7 has consistent correlation coefficients over most areas (Figure 3a). The CC of IMERGV05 has similar spatial pattern as that of 3B42V7, with slightly higher statistic values over most areas. 3B42V7 and IMERGV05 overestimate precipitation over most areas of Guangdong, especially for the central PRD and eastern mountainous area with high RB larger than 20% (Figure 3b,f). The distribution of RMSD shows similar spatial patterns with the total precipitation for the two estimates, and the values of RMSD for IMERGV05 are lower than 3B42V7 (Figure 3c,g). IMERGV05 exhibits much higher POD over the whole Guangdong Province (Figure 3h), indicating the improvement of IMERGV05 in detecting precipitation compared to 3B42V7. CMPA agrees well with gauge observations over most parts of Guangdong, with high CCs and PODs, and low RMSDs. The RBs of CMPA are generally small, characterized by an alternate distribution of positive and negative values.

Precipitation over Guangdong Province has significant variation in different seasons and regions with the effects of Monsoon climate. The precipitation centre is different in each season due to different rain types/formation (Figure 4). Rainfall in the first rainy season of Guangdong Province is mainly from the large-scale frontal system and accompanied with convective processes, especially from late-May to mid-June, when it is known as the "dragon-boat rain". The precipitation centre of the first rainy season is located over the north of PRD (ZQ, QY, and GZ) and the east coastal area (SW) (Figure 4n). The precipitation centres during the second rainy season (mainly for typhoon-related rainfall) are located over the west coastal area (ZJ, MM, YJ and ST) (Figure 4o).

Seasonal performances of 3B42V7 and IMERGV05 products over Guangdong Province and four sub-regions are summarized in Table 3. Overall, the regional and seasonal differences in the performance of 3B42V7 and IMERGV05 are large. During the whole period, 3B42V7 (and IMERGV05) demonstrates best performance over Reg1 (corresponds to the northern mountainous area) among the four sub-regions, with the highest CC of 0.66 (0.62) and relative small RMSD of 0.80 (0.64) mm, respectively. Meanwhile, metrics for 3B42V7 (IMERGV05) are worst over Reg4 (Reg3) with the smallest CC of 0.01 (largest RB of 14.87%). The poor performance of 3B42V7 (IMERGV05) over Reg4 (Reg3) is mainly attributed to the incapability in capturing precipitation during the JAS. 3B42V7 and IMERGV05 overestimate precipitation most with the higher RB (more than 10%) over Reg1 and Reg3.

IMERGV05 shows superiority over 3B42V7 in most conditions with higher CCs and smaller RBs and RMSDs, except for Reg3 during JAS with CC of 0.30 and RB of 23.21% (Table 3), and over Reg4 during OND with CC of 0.16. The improvement of IMERGV05 in detecting precipitation during JFM and AMJ (and during JAS over Reg4) is notable. While the bias of IMERGV05 is still obvious over Reg 3 (and over Reg1 during JFM and OND). Both

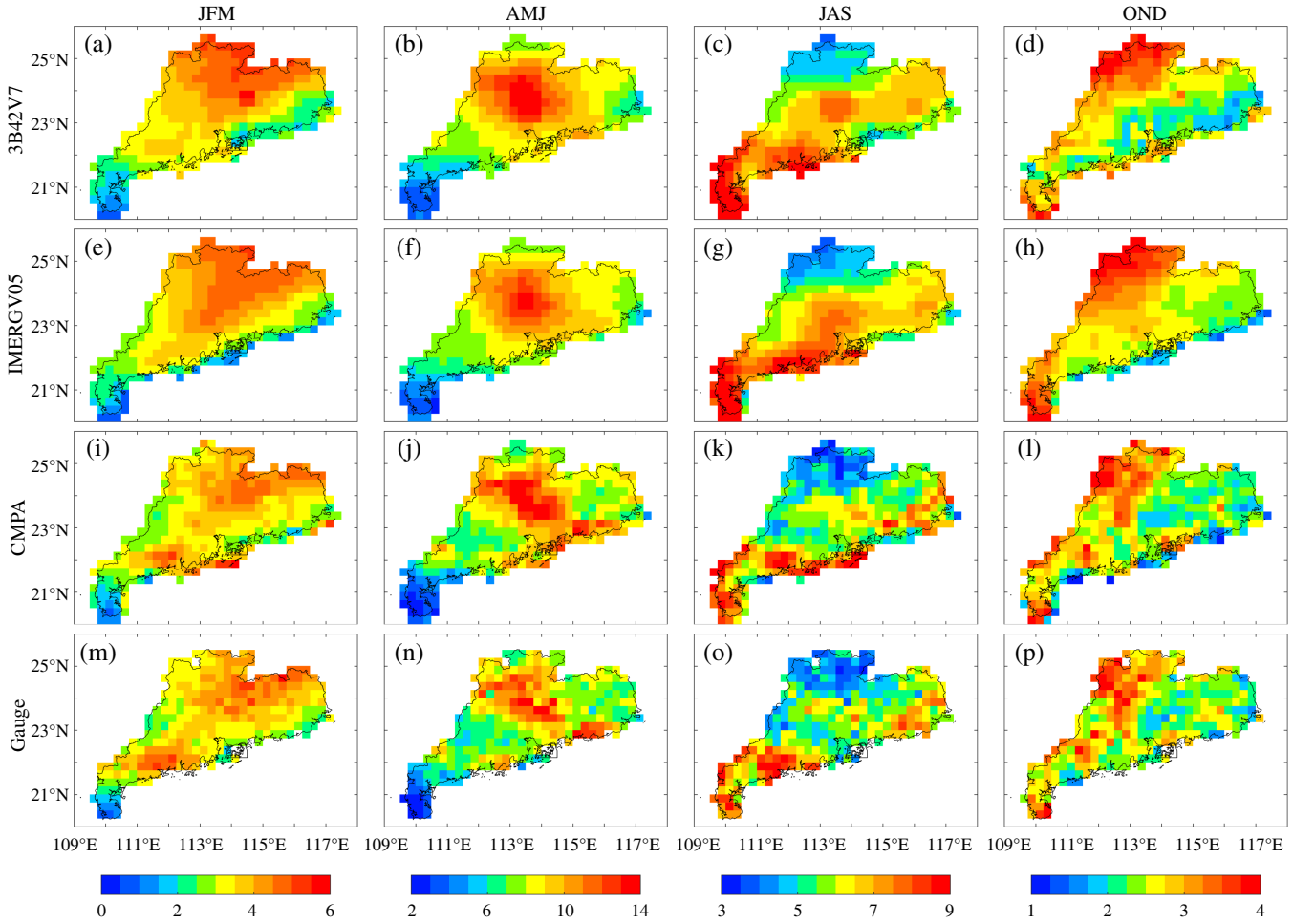

FIGURE 4 Seasonal mean precipitation (mm/day) distributions ranging from April 2014 to December 2016 derived from (a–d) 3B42V7, (e–h) IMERGV05, (i–l) CMPA and (m–p) gauge observation in Guangdong Province, China [Colour figure can be viewed at wileyonlinelibrary.com]

IMERGV05 and 3B42V7 show large overestimation over central PRD during JAS (Figure 4c,g). CMPA shows a good performance according to larger CC and smaller Bias during the whole period and four seasons (Table 3; Figure 4m–l).

IMERGV03 shows an abnormal blocky pattern in the central and eastern areas of Guangdong Province compared with its later version IMERGV04 and IMERGV05, and the blocky pattern mainly exists in JAS and OND (Figure 5). Meanwhile, IMERGV03 shows poorer performance than 3B42V7 and IMERGV04 with lower CCs (0.20 versus 0.55 and 0.51).

In general, 3B42V7 and IMERGV05 display seasonally dependent variations and have better performance during the rainy season and worse performance during the dry season (from October to the following March), as shown in Figure 6. This is consistent with the findings of Chen et al. (-Chen *et al.,* 2013a, 2013b). Over the whole Guangdong Province, the CC values show a large fluctuation; 3B42V7 and IMERGV05 fail to capture the spatial pattern of precipitation during December 2014, April 2015 and February 2016, with notably low CCs. Both products display significant positive RB values from April to July. CMPA demonstrates better performance in all months with higher CCs and lower RBs than 3B42V7 and IMERGV05.

3B42V7 severely underestimates the precipitation frequency for the light rainfall (rain rate <1 mm/day) (Figure 7a), but overestimates the relative frequency when rain rate exceeds 2 mm/day. Compared to 3B42V7, IMERGV05 greatly improves the ability to detect the light rain and heavy rain, and reasonably captures the frequency of precipitation with marginal overestimation. Underestimation in precipitation frequency occurs for the moderate rain (2–50 mm/day). When the rain rate is very large (>50 mm/day), IMERGV05 shifts to overestimate the frequency. IMERGV05 and 3B42V7 yield similar distribution patterns of rainfall volumes, both show underestimation in rain rate bins less than 20 mm/day and overestimation in rain rate bins over 50 mm/day. The PDF of daily precipitation is also reproduced by CMPA estimates, albeit showing minor overestimation in rain rates less than 0.5 mm/day and slight underestimation in rain rates between 2 and 20 mm/day.

IMERGV05 has larger CC, higher POD and CSI than 3B42V7 at the daily and 3-hr scale (Table 4). The metrics of IMERGV05 are greatly improved compared to 3B42V7 in

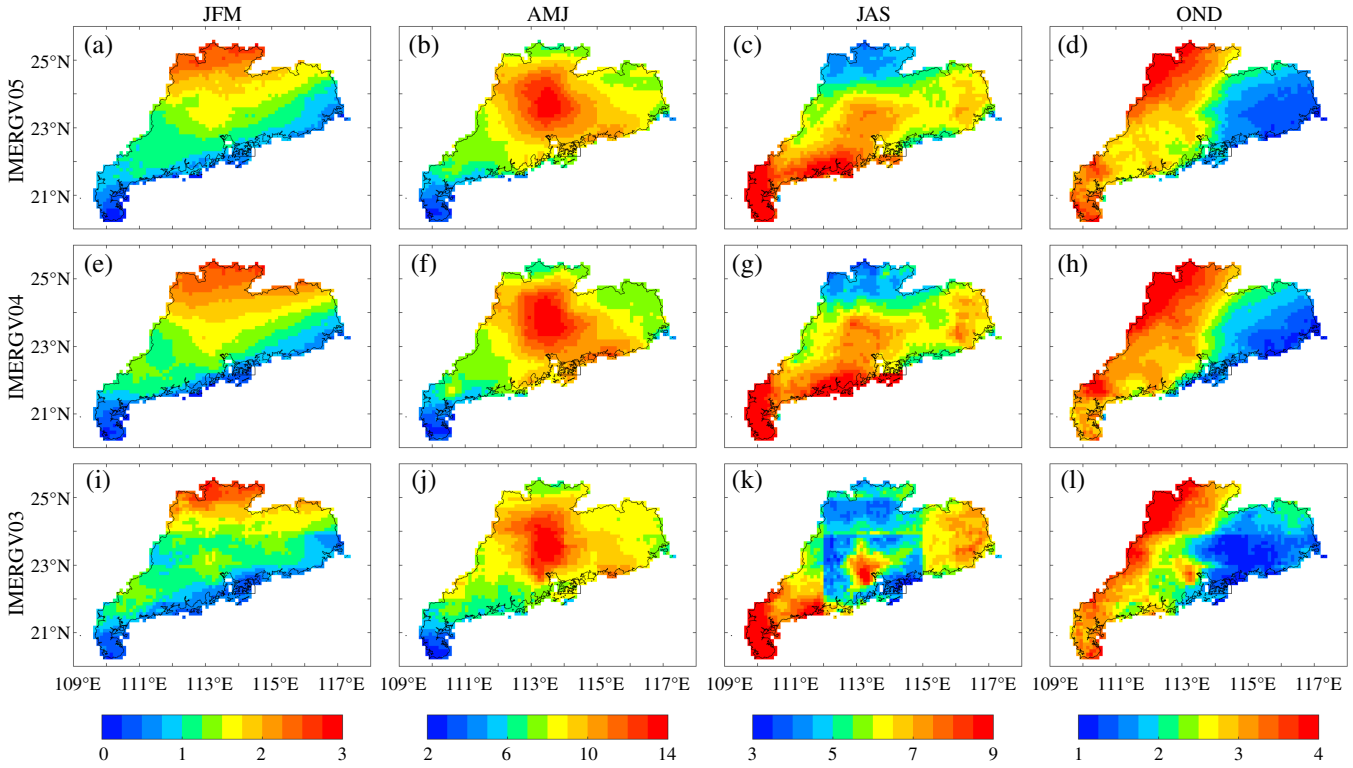

FIGURE 5 Seasonal mean precipitation (mm/day) distributions ranging from April 2014 to December 2015 derived from (a–d) IMERGV05, (e–h) IMERGV04 and (i–l) IMERGV03 in Guangdong Province, China. IMERGV03 displays an abnormal blocky spatial pattern during JAS and OND [Colour figure can be viewed at wileyonlinelibrary.com]

the 3-hr accumulation. This indicates that IMERGV05 could capture more precipitation hours correctly over Guangdong Province. On the other side, IMERGV05 shows higher FAR than that of 3B42V7 (~0.28 vs. ~0.13 at daily scale and ~0.46 vs. ~0.31 at 3-hr scale). The performance of IMERGV05 is better than IMERGV04 in terms of all metrics except POD in the daily and 3-hr scales evaluation (Table 4).

3.2 | Comparison of IMERG and CMPA at 0.1° grid

Both IMERGV05 and CMPA have higher frequency than gauges at the hourly scale when rain rate is less than 0.2 mm/hr and miss the occurrence of light rain (0.2–0.5 mm/hr) remarkably (Figure 7b). CMPA tends to detect more moderate rain between 0.5 and 2 mm/hr, and slightly underestimate rain larger than 2 mm/hr. IMERGV05 exhibits similar PDF features, with overestimation of the precipitation frequency between 0.5 and 5 mm/hr and underestimation when the rain rate is larger than 5 mm/hr. CMPA over-detects moderate precipitation amount (rain rate between 1 and 10 mm/hr) and underestimates the volume of precipitation of heavy rain (>20 mm/hr) (Figure 7d). Overall, IMERGV05 could well reveal the precipitation occurrence pattern at the hourly scale, even comparable with CMPA product.

The data quality of IMERGV05 at the hourly and 0.1° scale has some limitations. CMPA has higher CC, POD and CSI and lower RB, RMSD and FAR than those of IMERGV04 and IMERGV05 in Guangdong Province, China (Table 4). All the metrics (except for FAR) are reduced as the temporal resolution decreased from daily to hourly for IMERG. Besides, the gaps of POD and CSI between IMERGV05 (0.59 and 0.32) and CMPA (0.81 and 0.52) are large. IMERGV05 shows improvement in data quality compared with IMERGV04 with lower bias/RMSD and higher CSI. Both products show high FAR values at the hourly scale, indicating that the algorithms used in IMERGV05 and CMPA still have limitation in detecting light rain. On the other hand, light rain may evaporate rapidly and not be observable by the ground gauges.

The gauge observations show a two-peak diurnal feature during the first-rainy season, with the stronger one around 16:00 and another in the morning (Figure 8a–d). The minimum rainfall is all observed at midnight. CMPA generally captures the diurnal pattern of precipitation, but with some considerable overestimation in Reg1 and Reg3. IMERGV05 also can reproduce the diurnal structure of precipitation over the four sub-regions, while with a larger overestimation for the afternoon peak than CMPA.

Unlike the first rainy season, the dominant feature in the second rainy season is a single strong peak during 15:00 to 17:00 LST (Figure 8e–h). IMERGV05 captures the diurnal features from midnight to noon but shows large overestimation from afternoon to evening. IMERGV05 is more fluctuating in Reg3 than others (Figure 8c,g). In general, CMPA

TABLE 3 Summary of evaluation metrics for 3B42V7, IMERGV05 and CMPA products in Guangdong Province and four sub-regions

	CC			RB (%)			RMSD (mm)		
	3B42V7	IMERGV05	CMPA	3B42V7	IMERGV05	CMPA	3B42V7	IMERGV05	CMPA
Guangdong	0.48	0.51	0.74	9.71	9.31	3.13	0.85	0.80	0.55
Reg1	0.66	0.62	0.76	12.82	8.62	3.43	0.80	0.64	0.47
Reg2	0.58	**0.47**	0.76	6.65	7.31	−1.02	0.69	0.75	0.51
Reg3	0.44	0.51	0.70	**13.89**	**14.87**	6.51	1.03	1.01	0.63
Reg4	**0.01**	0.28	0.64	3.19	3.56	1.79	0.76	0.62	0.52
JFM									
Guangdong	0.70	0.73	0.88	2.54	3.34	−1.63	0.71	0.62	0.39
Reg1	0.57	0.70	0.85	**20.10**	**14.93**	0.79	0.90	0.70	0.29
Reg2	0.71	0.78	0.89	−9.87	−9.16	−7.67	0.77	0.72	0.52
Reg3	0.53	0.55	0.81	2.22	5.08	0.28	0.64	0.63	0.37
Reg4	0.92	0.90	0.88	−4.83	−0.55	−1.67	0.45	0.36	0.36
AMJ									
Guangdong	0.78	0.81	0.90	12.34	9.32	7.42	1.78	1.52	1.20
Reg1	0.73	0.73	0.82	10.85	4.71	5.54	1.57	1.19	1.22
Reg2	0.87	0.85	0.94	12.48	12.16	4.09	1.17	1.20	0.70
Reg3	0.64	0.70	0.84	**18.26**	**14.34**	11.60	2.29	1.93	1.50
Reg4	**0.37**	0.61	0.83	4.55	4.50	5.51	1.66	1.43	1.07
JAS									
Guangdong	0.73	0.68	0.78	13.22	12.72	1.19	1.18	1.23	0.83
Reg1	0.49	0.39	0.64	14.42	10.79	1.98	0.88	0.84	0.56
Reg2	0.69	0.64	0.76	10.44	8.92	−3.47	1.25	1.27	0.98
Reg3	0.42	**0.30**	0.46	**19.91**	**23.21**	5.08	1.41	1.61	0.88
Reg4	**0.21**	0.49	0.62	6.37	4.06	0.77	0.97	0.80	0.80
OND									
Guangdong	0.50	0.60	0.82	1.00	7.18	−0.70	0.52	0.48	0.33
Reg1	0.58	0.63	0.81	10.09	**11.49**	1.63	0.54	0.54	0.34
Reg2	**0.15**	0.32	0.73	−2.11	5.79	−0.31	0.56	0.56	0.41
Reg3	**0.07**	0.45	0.79	−2.68	7.05	−0.85	0.53	0.43	0.28
Reg4	0.30	**0.16**	0.70	−1.15	3.44	−4.02	0.41	0.38	0.27

Note. The metrics were calculated based on the mean daily precipitation from April 2014 to December 2016 at 0.25° grid. The notable differences between these products are highlighted with bold font.

fits the diurnal cycles well in all regions and shows its capability in representing hourly precipitation features.

3.3 | Decomposition of bias into error components

The magnitudes of total bias derived from 3B42V7 and IMERGV05 are similar and are larger than that of CMPA (Figure 9a–c; Table 5), which is consistent with the statistical metrics shown in Figure 2 and Table 3. 3B42V7 shows large overestimation in mountainous areas and PRD (Figure 9a). Total biases consist of the positive hit bias (overestimation, Figure 9d), and the false precipitation (Figure 9j), while offsetting by the missed precipitation (Figure 9g). Notable underestimation takes place over the two coastal precipitation centres of Guangdong, which could be traced to large missed precipitation (Figure 9g). The missed components are largely caused by the failure in detecting convective thunderstorms and typhoon-related rainfall during the rainy season and rainfall during the dry period (Figure 10c). The large amount of missed precipitation records of 3B42V7 are the main reason for the poor performance in POD (Figure 3d), and the missed precipitation is reduced remarkably in IMERGV05 (Figure 10c).

The error features of IMERGV05 have similar spatial patterns with 3B42V7, having remarkable overestimation over central PRD and underestimation in the surrounding areas (Figure 9b). These overestimations are attributed primarily to large hit bias (Figure 9e; Table 5), with secondary contribution from the positive false precipitation (Figure 9k). The underestimation over the two coastal precipitation centres is dominated by negative hit bias and missed precipitation (Figure 9e,h). IMERGV05 fails to detect several heavy rainfall events over YJ city during the rainy season.

CMPA shows slight overestimation of precipitation in PRD, and underestimation over the western mountainous region (Figure 9c). Its total bias is characterized by an interleaved distribution of small positive and negative values over inland areas. Both the overestimates and underestimates are mostly from hit bias (Figure 9f). Missed precipitation is negligible for CMPA, while the false precipitation for CMPA

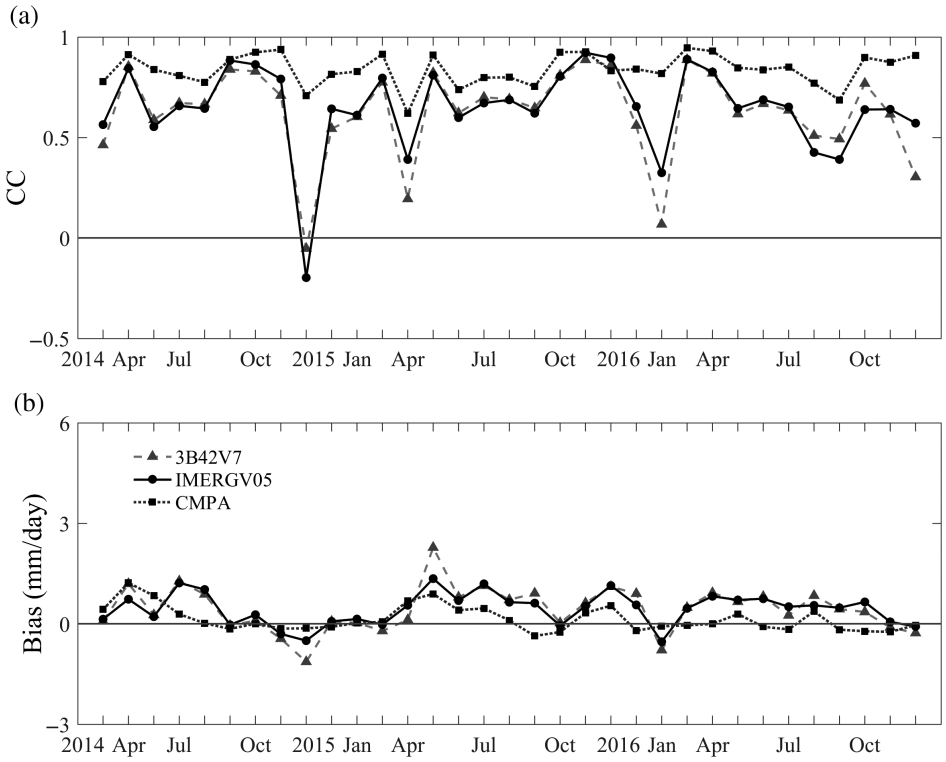

FIGURE 6 Monthly series of CC and bias between 3B42V7, IMERGV05 and CMPA products and gauges observations in the entire Guangdong Province

is not negligible, which may be caused by the retrieval algorithms of the raw CMORPH data (Figure 9l; Table 5).

Generally, total bias and hit bias are higher during the rainy season and lower during the dry season, except for the end of January 2016 when an extreme precipitation event stroke Guangdong Province (Figure 10a,b). The total bias of the two rainy seasons is positive, with dominant source of hit bias and false precipitation (Figure 10b,d). The large false components may mainly accord to the false detection of the cloud that doesn't rain. In the dry period, CMPA tends to underestimate precipitation, mainly attributing to a shift of hit bias from positive to negative (Figure 10b).

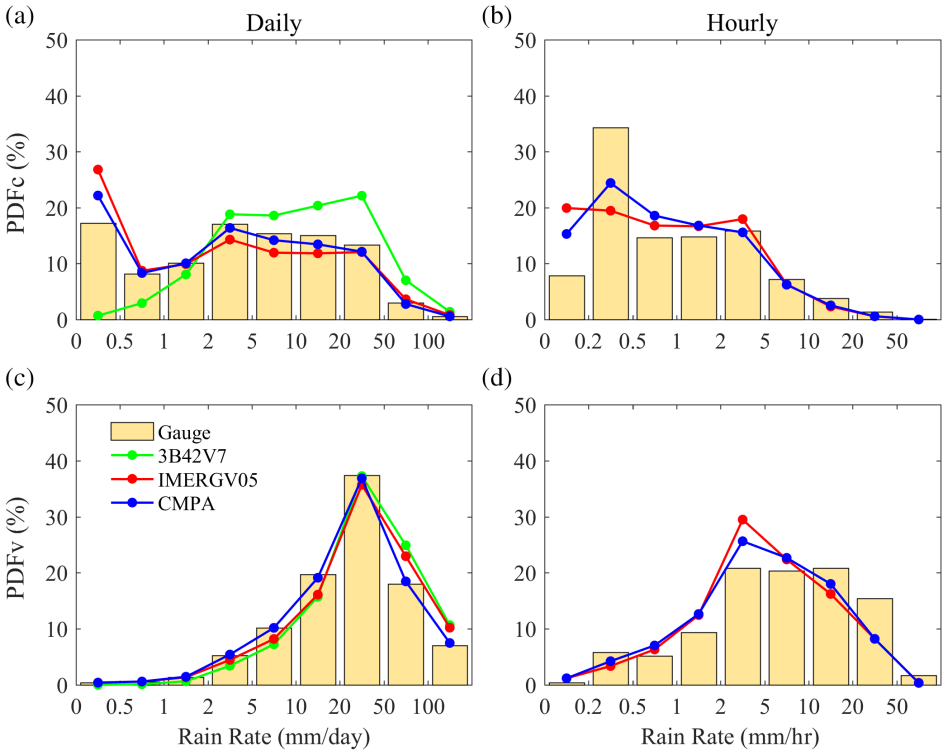

FIGURE 7 Probability distribution function by occurrence of daily and hourly precipitation (a and b) and by volume (c and d) with different rain intensity intervals in the Guangdong Province [Colour figure can be viewed at wileyonlinelibrary.com]

TABLE 4 Summary of evaluation metrics for 3B42V7, IMERGV04, IMERGV05 and CMPA products in daily and 3-hr accumulation and at the 0.25° grid in the Guangdong Province, China

	Product	CC	Bias (mm)	RMSD (mm)	POD	FAR	CSI
Daily	3B42V7	0.67	0.98	15.64	0.56	0.13	0.52
	IMERGV04	0.72	0.94	13.63	0.84	0.32	0.61
	IMERGV05	0.75	0.80	12.25	0.82	0.28	0.62
	CMPA	0.89	0.29	7.81	0.92	0.18	0.77
3-hr	3B42V7	0.30	0.30	8.18	0.31	0.31	0.27
	IMERGV04	0.57	0.24	5.46	0.69	0.51	0.40
	IMERGV05	0.59	0.21	4.99	0.66	0.46	0.42
	CMPA	0.80	0.08	3.49	0.86	0.30	0.62
Hourly	IMERGV04	0.35	0.13	3.97	0.63	0.64	0.30
	IMERGV05	0.35	0.12	3.86	0.59	0.59	0.32
	CMPA	0.64	0.03	3.11	0.81	0.41	0.52

Notes. The hourly comparison between IMERGV05, IMERGV04 and CMPA is carried out at the 0.1° grid. The metrics were calculated based on grids with at least one rain gauge.

Distributions of total precipitation with intensity show difference among the three products (Figure 11a–c). 3B42V7 constantly underestimates the total precipitation when the rain rate is less than 10 mm/day but turns to overestimate afterwards. The low frequency of light precipitation (<1 mm/day) is seen in both hit bias and false precipitation by 3B42V7, which is consist with the PDF patterns in Figure 7, leading to underestimation of precipitation in this range. This is reasonable since the PMW radiometers in the TRMM-era are less sensitive to the light rain in most conditions. Besides light rain, the missed component of 3B42V7 also happens for the moderate rain between 1 and 20 mm/hr (Figure 11g). IMERGV05 matches well with the distribution of gauge observations when the rain rate is less than 10 mm/day, and overestimate for rain rate larger than 20 mm/day (Figure 11b). The overestimation of the heavy rain (>50 mm/day) for 3B42V7 and IMERGV05 mainly comes from the hit bias that falsely estimates the precipitation from moderate intensity to heavier rainfall (Figure 11d–e). The similar frequency patterns are seen in hit bias by both 3B42V7 and IMERGV05, while IMERGV05 notably reduces the amount of hit bias. The distribution of CMPA in total precipitation matches well with the gauge observations (Figure 11c).

Generally, the variations of hit bias for different products are similar, with overestimations for light rain and underestimations for heavy rain (Figure 11d–f), which is also observed by other researches (Chen *et al.,* 2013a; Chen *et al.,* 2013b; Wang *et al.,* 2016). All products considerably overestimate the moderate rain of 5–20 mm/day. Most

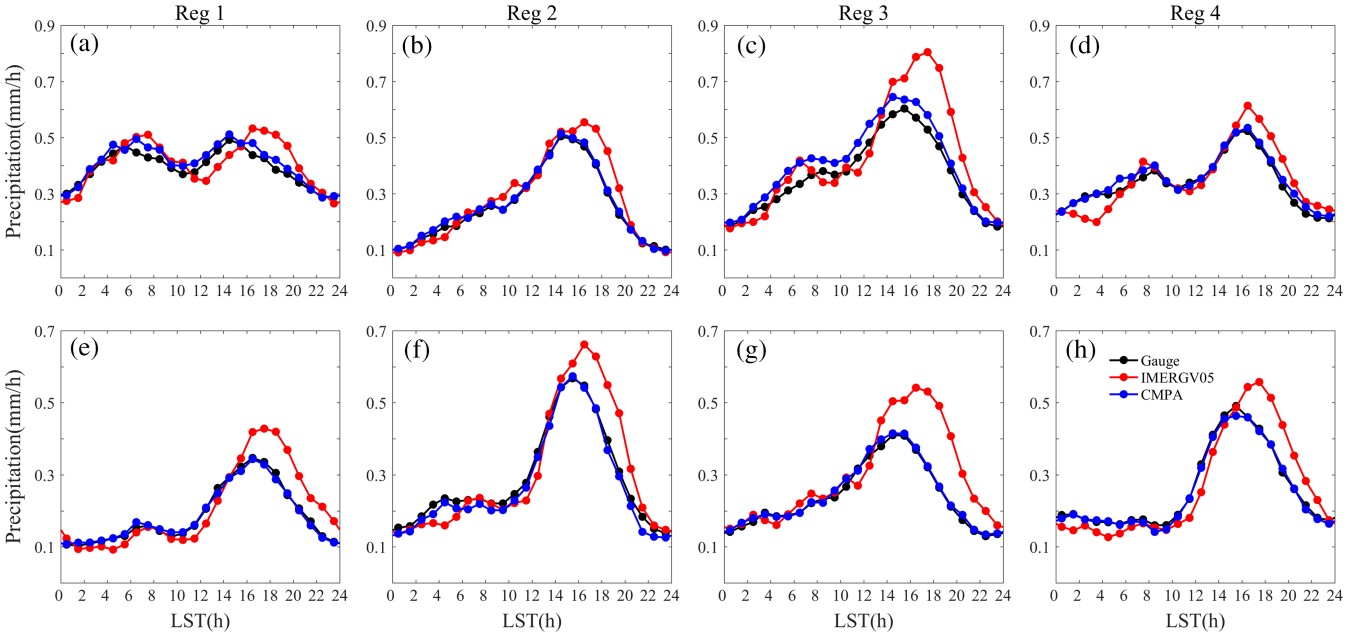

FIGURE 8 Diurnal cycle of precipitation in the four sub-regions during the first rainy season (April–June, a–d) and the second rainy season (July–September, e–h). The diurnal cycles were calculated based on the hourly and areal mean precipitation and converted to the local solar time (GMT + 8) [Colour figure can be viewed at wileyonlinelibrary.com]

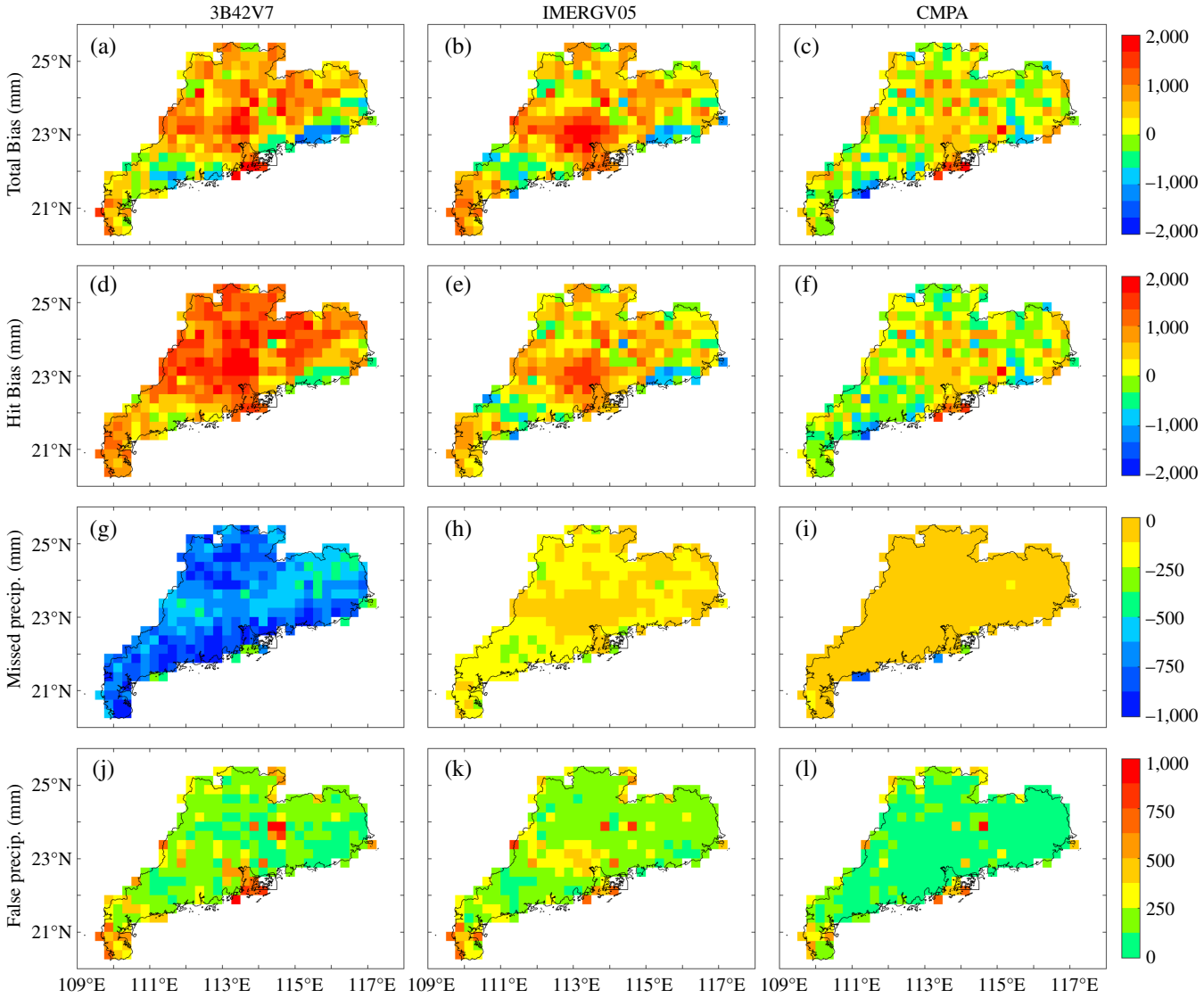

FIGURE 9 Spatial variabilities of the total bias (E, a–c) and the three bias components: Hit bias (H, d–f), missed precipitation (M, g–i) and false precipitation (F, j–l) of the three products. The biases were computed using the daily precipitation series at each grid ranging from April 2014 to December 2016. The relationship between them is E = H-M + F [Colour figure can be viewed at wileyonlinelibrary.com]

missed and false precipitation occurs in light rain (<0.5 mm/day), expect for the false precipitation of 3B42V7 (Figure 11g–l).

4 | DISCUSSION

Some efforts have been made to compare the performance of different satellite-based precipitation estimates. These products tend to underestimate (overestimate) the amount of heavy (light) rainfall (Chen *et al.,* 2013b; Mei *et al.,* 2014). Their performance has seasonal variation with better abilities during the warm season than in the cold season (Chen *et al.,* 2013a; Chen *et al.,* 2013b). These products may fail in detecting the rain, or they generate inaccurate estimates of the rainfall intensity (Sunilkumar *et al.,* 2015). Our results are generally consistent with their findings. Notable underestimation takes place over the two coastal precipitation centres for 3B42V7, and the underestimation is primarily from the missed precipitation, and secondarily from the negative hit bias (Figure 9a,d,g). Other studies also demonstrated that the occurrence and amount of precipitation tend to be underestimated by 3B42 estimates over some coastal areas (e.g., McCollum *et al.,* 2002; Melo et al., 2015; Tang *et al.,* 2015). This issue may be due to the lack of capability to capture the warm rain process and convective rainfall and the surface emissivity effects of PMW radiometers in the

TABLE 5 The spatial mean values of the total bias and the three bias components of the three products (mm/day), and the relative contribution of the three components to total bias (%)

	3B42V7	IMERGV05	CMPA
Total bias	0.49	0.48	0.16
Hit bias	0.98 (198%)	0.39 (82%)	0.07 (44%)
Missed precipitation	−0.72 (−146%)	−0.15 (−31%)	−0.04 (−25%)
False precipitation	0.24 (48%)	0.24 (49%)	0.13 (81%)

The biases were accumulated from April 2014 to December 2016 at 0.25° grid.

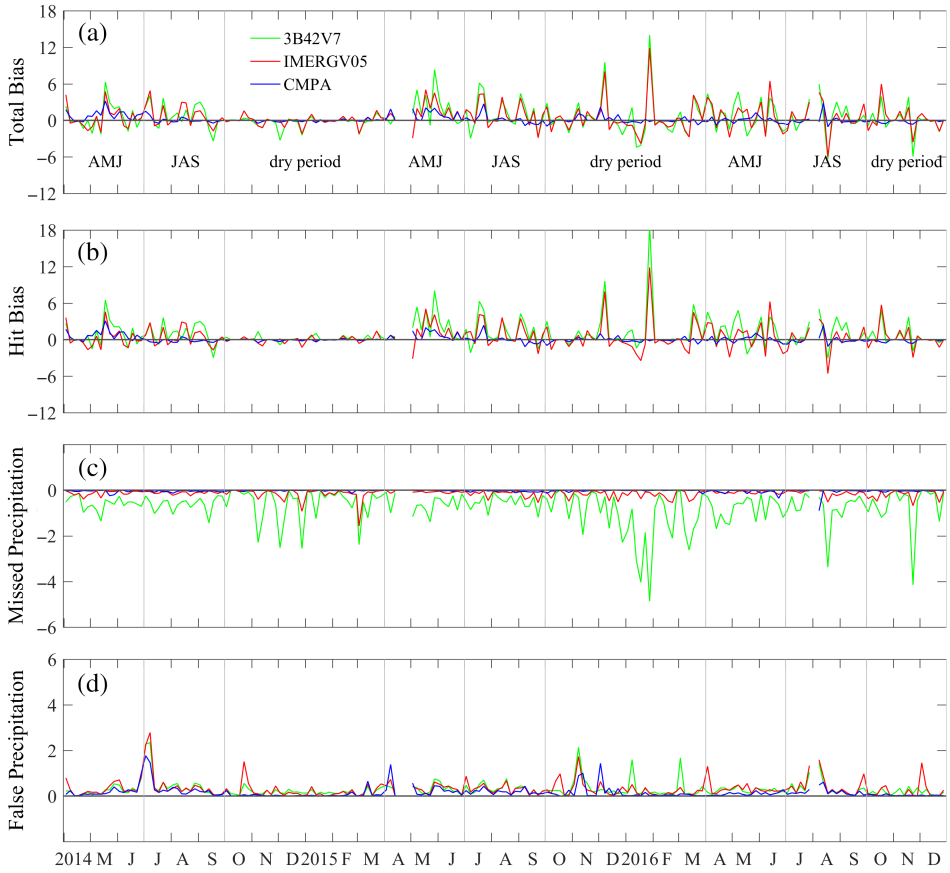

FIGURE 10 Daily series of the total bias (a) and the three bias components: hit bias (b), missed precipitation (c) and false precipitation (d) (area average, in mm/day) of the three products over the Guangdong Province. A 5 days average is applied for smoothing the series [Colour figure can be viewed at wileyonlinelibrary.com]

transition zones from ocean to land (Michaelides *et al.,* 2009; Tian *et al.,* 2009). Obviously, IMERGV05 does not overcome this issue, and the underestimation is mainly attributed by negative hit bias (Figure 9e). These results highlight the necessity of evaluation work over coastal areas to have comprehensive understanding of error features in the IMERG-era.

IMERGV05 significantly improves the ability to detect the light rain and heavy rain compared with 3B42V7 for the daily accumulation (Figure 7). The improvement of IMERGV05 in detecting precipitation is more remarkable for the 3-hr accumulation. IMERGV05 has higher CC, POD and CSI values and lower RMSD at almost all regions than the metrics of 3B42V7 (Table 4). In addition, the results of errors decomposition indicate that the improvement of IMERGV05 in error reduction is notable in reducing the amplitude of hit bias and missed precipitation compared to 3B42V7 (Figures 9–11). Attention must be paid that point-grid comparison may cause some uncertainty due to the large grid size of ~25 km. Since we could not add more rain gauges although the present rain gauges are relatively dense (one gauge per 100 km^2 on average), our solution is to validate the satellite rainfall in different spatial resolution (0.1° and 0.25° grids) and temporal accumulations (hourly, 3-hr, daily, monthly and annual). The longer temporal accumulation and larger spatial average normally generate better agreement.

Several studies have highlighted that the former version of IMERG (IMERGV03) has greatly improved the performance in capturing the precipitation than the TMPA 3B42 (Guo *et al.,* 2016; Prakash *et al.,* 2016; Tang *et al.,* 2016). However, IMERGV03 displays an abnormal blocky spatial pattern in PRD, significantly overestimating precipitation over the central PRD while underestimating precipitation in the surrounding areas (Figure 5e–h). The messy spatial distribution of precipitation of IMERGV03 over Reg3 is likely due to a known problem that occurs in the combination of the multi-satellite data (personal contact with Dr. George Huffman). Since the sampling estimates from a single GPM core is limited, the IMERG is designed to use as many PMW sensors from multiple LEO satellites as possible, and then fills the gaps using estimates from geostationary satellite IR sensors. Thus, due to the limited sampling of original data, the errors for the propagated PMW estimates may be regionally dependent and seasonally changing by the sensor type, and no smoothing is applied when splicing the target grid box together (Huffman *et al.,* 2015). The blocky pattern is also found in the 3B42V7 (though it is not obvious) and the IMERGV03 UnCal estimates. Nevertheless, as shown in our study, this problem has been corrected in its later version

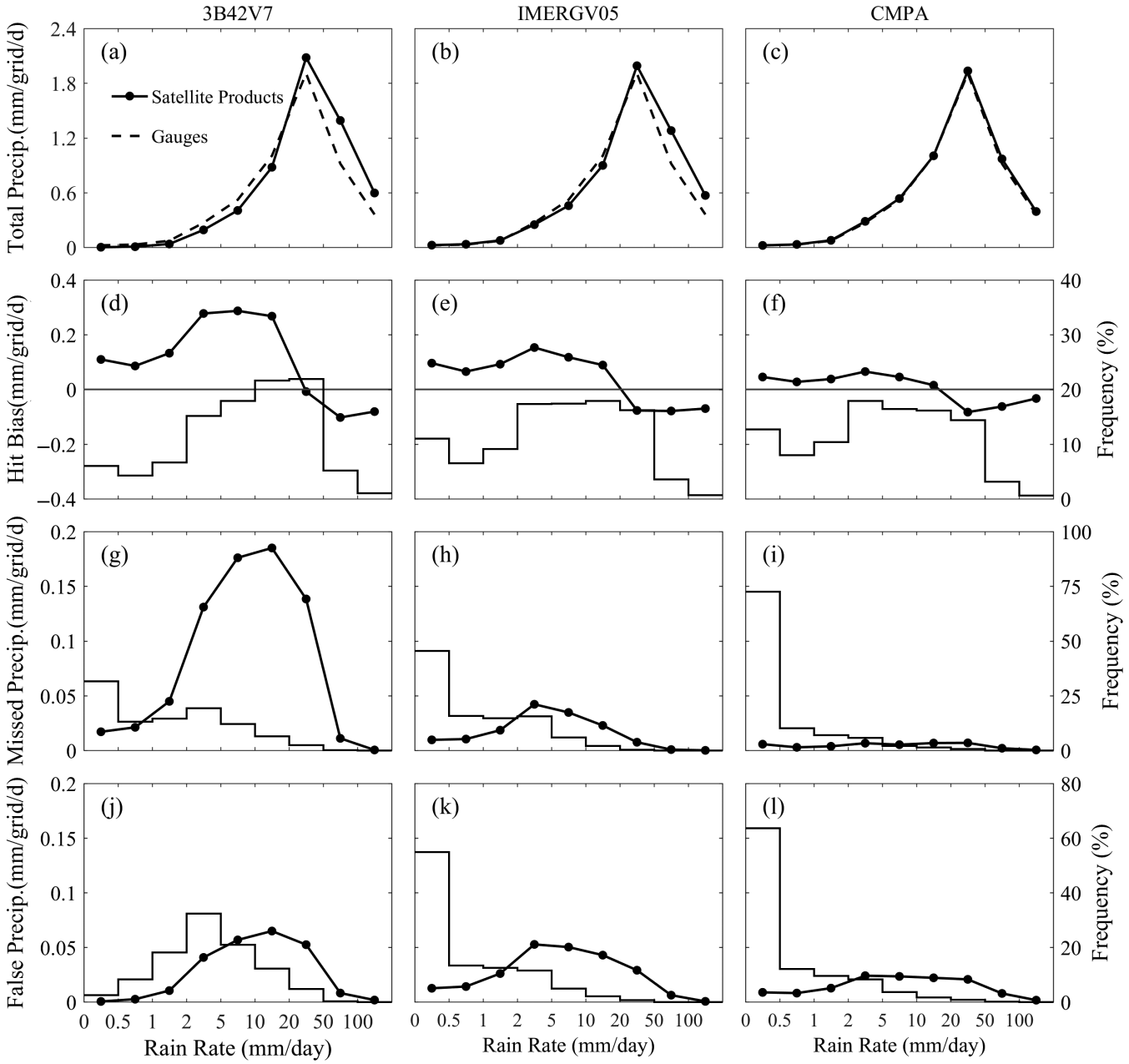

FIGURE 11 Intensity distributions of the total precipitation for the three products and gauges with different rain rate intervals over the Guangdong Province (a–c); intensity distributions (lines, left-hand vertical axis) and frequency distributions (stairs, right-hand vertical axis) of the hit bias (d–f), missed precipitation (g–i), and false precipitation (j–l) for the three products with different rain rate intervals

of IMERGV04 which also addresses a number of issues uncovered in IMERGV03. Besides, the latest version IMERGV05 has further improved data quality compared with IMERGV04 with higher CC, CSI and lower Bias, RMSD and FAR (Table 4).

IMERGV05 has some limitations for its hourly/half-hour accumulations (Table 4). Compared with other sub-regions, Reg3 has much more fluctuating diurnal features for all estimates, indicating the limitation in reproducing the hourly precipitation characteristics over the low-lying coastal region (Figure 8c,g). IMERGV05 and CMPA tend to detect more frequency of light rain and moderate rain (Figure 7), which may be partially due to the overestimation to the amount of light rain and underestimation to the amount of the heavy rain. This is a common challenge for satellite-based precipitation products (Mei *et al.,* 2014; Wang *et al.,* 2016). Overall, CMPA agrees well with gauge observations and outperforms both 3B42V7 and IMERG estimates in most regions and scales, CMPA could be used as a reference for validating other satellite precipitation products.

The data quality of satellite precipitation estimates has great enhancement after bias-correction using rain gauge observations. Both 3B42V7 and IMERG products were corrected at 1°× 1° grids by the monthly precipitation from

GPCC gauges. However, GPCC only include 194 China's International Exchange Stations over mainland China (Tang *et al.,* 2016), and only six stations are in the Guangdong Province (Figure 1a), which are quite sparse. In contrast, CMPA integrates the hourly gauge observations from more than 30,000 automatic weather stations maintained by the China Meteorology Administration in mainland China. In addition, both 3B42V7 and IMERG products are adjusted with monthly gauge observations, while CMPA is merged with hourly gauge data. Moreover, precipitation often demonstrates strong spatiotemporal variation over mountainous areas and urban areas. For example, Guangzhou (station 59,287) usually had more precipitation than its surrounding areas during rainy season (Wang *et al.,* 2018). Urban environments probably play a positive role in generating the short-duration heavy precipitation and cause uneven spatial distribution over central PRD (Figure 4n,o). Therefore, the strong positive bias of IMERGV05 and 3B42V7 is likely related to the bias correction that used the precipitation of station 59,287 to adjust data over the entire PRD area (Figure 4c,g). The difference in gauge adjustment between 3B42V7/IMERG and CMPA may be the key for their different performance. Generally, CMPA estimate presents good performance (Shen *et al.,* 2014; Wang *et al.,* 2016) and has been employed to analyse the precipitation characteristics of China (Chen *et al.,* 2016a; Chen *et al.,* 2016b).

The rainfall data used in this study are from the gauge network maintained by the Department of Water Resource in Guangdong Province, China. Physically, these rain gauges are different from those of China Meteorology Administration, and thus would be an independent analysis of the CMPA validation. Nevertheless, some rain gauges used in this study might be located closely to those used in CMPA, thus showing better performances for CMPA validation. In other words, the better performance of CMPA over other global products is partially due to the inclusion of hourly rain gauges data, even if the rain gauges used for validation are not physically the same instruments used for building CMPA, but located in the neighbourhood area. In addition, the density of the rain gauge used in CMPA also affects the quality of CMPA estimates. The good performance of CMPA in Guangdong Province depends on its high density of rain gauges used, CMPA may perform differently in other provinces due to their different density/distribution of available rain gauges (Xie and Xiong, 2011; Shen *et al.,* 2014).

5 | CONCLUSIONS

Three satellite-based precipitation estimates have been comprehensively evaluated against the hourly precipitation observations from a dense rain gauge network in the Guangdong Province, Southern China from April 2014 to December 2016. The important conclusions are summarized below.

1. IMERGV05 greatly reduces the hit bias and missed precipitation of 3B42V7, thus showing better ability in detecting the light rain and heavy rain.
2. IMERGV05 shows better performance than IMERGV03 and IMERGV04, especially solving the problem of an abnormal blocky pattern of IMERGV03 in the Pearl River Delta area.
3. IMERGV05 still has some limitations for its hourly/half-hour accumulation compared to CMPA. IMERGV05 could improve the capability in reducing its false detection and reconstructing the diurnal cycle, particularly for the overestimation problem from afternoon to midnight during the rainy season.
4. CMPA shows much smaller bias than in IMERGV05 and 3B42V7, and could recover the hourly precipitation recorded by dense gauge measurements in the Guangdong Province of southern China. CMPA may work as a reference to validate other satellite precipitation products in Guangdong Province and may perform differently in other provinces.
5. 3B42V7 and IMERGV05 have large areas of overestimation in the mountainous areas and underestimation in the coastal areas, while CMPA is characterized by an alternate distribution of small positive and negative values. The overestimation of precipitation is partially attributed to the positive hit biases that falsely estimate the precipitation from moderate intensity to heavier rainfall by the three products.

ACKNOWLEDGEMENTS

This study is funded by the Water Resource Science and Technology Innovation Program of Guangdong Province (#2016-19), National Natural Science Foundation of China (#51779278), Science and Technology Program of Guangzhou (#1561000154; #201707010098), Guangdong Research Station of Science and Technology Experts (2015A090905002). The authors acknowledge Dr. George J. Huffman at NASA Goddard Space Flight Center for consulting the IMERG information and the Department of Water Resources in Guangdong Province for providing the gauge observations. Comments and suggestions provided from the editor and two reviewers greatly improve this manuscript and are highly appreciated.

ORCID

Dashan Wang http://orcid.org/0000-0001-9743-4806

REFERENCES

Arkin, P.A. and Xie, P.P. (1994) The global precipitation climatology project: first algorithm Intercomparison project. *Bulletin of the American Meteorological Society*, 75, 401–419. https://doi.org/10.1175/1520-0477(1994)075<0401:TGPCPF>2.0.CO;2.

Chen, S., Hong, Y., Cao, Q., Gourley, J.J., Kirstetter, P., Yong, B., Tian, Y.D., Zhang, Z., Shen, Y., Hu, J. and Hardy, J. (2013a) Similarity and difference

of the two successive V6 and V7 TRMM multisatellite precipitation analysis performance over China. *Journal of Geophysical Research: Atmospheres*, 118, 13,060–13,074. https://doi.org/10.1002/2013JD019964.

Chen, S., Hong, Y., Gourley, J.J., Huffman, G.J., Tian, Y.D., Cao, Q., Yong, B., Kirstetter, P., Hu, J., Hardy, J., Li, Z., Khan, S.I. and Xue, X. (2013b) Evaluation of the successive V6 and V7 TRMM multisatellite precipitation analysis over the continental United States. *Water Resources Research*, 49, 8174–8186. https://doi.org/10.1002/2012WR012795.

Chen, S., Tian, Y., Behrangi, A., Hu, J., Hong, Y., Zhang, Z., Stepanian, P., Hu, B. and Zhang, X. (2016a) Precipitation spectra analysis over China with high-resolution measurements from optimally-merged satellite/gauge observations—part I: spatial and seasonal analysis. *IEEE J-STARS*, 9, 2966–2978. https://doi.org/10.1109/JSTARS.2016.2529003.

Chen, S., Behrangi, A., Tian, Y., Hu, J., Hong, Y., Tang, Q., Hu, X., Stepanian, P., Hu, B. and Zhang, X. (2016b) Precipitation spectra analysis over China with high-resolution measurements from optimally-merged satellite/gauge observations—part II: diurnal variability analysis. *IEEE J-STARS*, 9, 2979–2988. https://doi.org/10.1109/JSTARS.2016.2529001.

Dai, A., Lin, X. and Hsu, K. (2007) The frequency, intensity, and diurnal cycle of precipitation in surface and satellite observations over low- and mid-latitudes. *Climate Dynamics*, 29, 727–744. https://doi.org/10.1007/s00382-007-0260-y.

Ebert, E.E., Janowiak, J.E. and Kidd, C. (2007) Comparison of near-real-time precipitation estimates from satellite observations and numerical models. *Bulletin of the American Meteorological Society*, 88, 47–64.

Ferraro, R.R. (1997) Special sensor microwave imager derived global rainfall estimates for climatological applications. *Journal of Geophysical Research*, 102, 16,715–16,735. https://doi.org/10.1029/97JD01210.

Gao, Y. and Liu, M. (2013) Evaluation of high-resolution satellite precipitation products using rain gauge observations over the Tibetan Plateau. *Hydrology and Earth System Sciences*, 17, 837–849.

GPM Science Team. (2018). Integrated Multi-satellitE Retrievals for GPM (IMERG), version 05B. NASA Goddard Earth Science Data and Information Services Center. Available at: ftp://arthurhou.pps.eosdis.nasa.gov/gpmdata/ [Accessed January 2018]

Guo, H., Chen, S., Bao, A., Behrangi, A., Hong, Y., Ndayisaba, F., Hu, J. and Stepanian, P.M. (2016) Early assessment of integrated multi-satellite retrievals for global precipitation measurement over China. *Atmospheric Research*, 176–177, 121–133. https://doi.org/10.1016/j.atmosres.2016.02.020.

Hossain, F. and Huffman, G.J. (2008) Investigating error metrics for satellite rainfall data at hydrologically relevant scales. *Journal of Hydrometeorology*, 9, 563–575. https://doi.org/10.1175/ 2007JHM925.1.

Hossain, F. and Lettenmaier, D.P. (2006) Flood prediction in the future: recognizing hydrologic issues in anticipation of the global precipitation measurement mission. *Water Resources Research*, 42, W11301. https://doi.org/10.1029/2006WR005202.

Hou, A.Y., Kakar, R.K., Neeck, S.P., Azarbarzin, A.A., Kummerow, C.D., Kojima, M., Oki, R., Nakamura, K. and Iguchi, T. (2014) The global precipitation measurement mission. *Bulletin of the American Meteorological Society*, 95, 701–722.

Huffman, G.J., Adler, R.F., Bolvin, D.T., Gu, G., Nelkin, E.J., Bowman, K.P., Stocker, E.F. and Wolff, D.B. (2007) The TRMM multi-satellite precipitation analysis: quasi-global, multi-year, combined-sensor precipitation estimates at fine scale. *Journal of Hydrometeorology*, 8, 33–55. https://doi.org/10.1175/JHM560.1.

Huffman GJ, Bolvin DT, Braithwaite D, Hsu K, Joyce R. 2015. *Algorithm Theoretical Basis Document (ATBD) Version 4.5: NASA Global Precipitation Measurement (GPM) Integrated Multi-satellitE Retrievals for GPM (IMERG).* NASA: Greenbelt, MD, p. 26. https://pmm.nasa.gov/sites/default/files/document_files/IMERG_ATBD_V4.5.pdf

Huffman GJ, Bolvin DT, Braithwaite D, Hsu K, Joyce R, Kidd C, Nelkin EJ, Sorooshian S, Tan J, Xie P. 2018. *Algorithm Theoretical Basis Document (ATBD) Version 5.2 for the NASA Global Precipitation Measurement (GPM) Integrated Multi-satellitE Retrievals for GPM (I-MERG).* GPM Project: Greenbelt, MD, p. 36. https://pmm.nasa.gov/sites/default/files/document_files/IMERG_ATBD_V5.2.pdf

Jiang, S., Ren, L., Hong, Y., Yong, B., Yang, X., Yuan, F. and Ma, M. (2012) Comprehensive evaluation of multi-satellite precipitation products with a dense rain gauge network and optimally merging their simulated hydrological flows using the Bayesian model averaging method. *Journal of Hydrology*, 452, 213–225. https://doi.org/10.1016/j.jhydrol.2012.05.055.

Joyce, R.J., Janowiak, J.E., Arkin, P.A. and Xie, P.P. (2004) CMORPH: a method that produces global precipitation estimates from passive microwave and infrared data at high spatial and temporal resolution. *Journal of Hydrometeorology*, 5, 487–503.

Kidd, C. and Levizzani, V. (2011) Status of satellite precipitation retrievals. *Hydrology and Earth System Sciences*, 15, 1109–1116. https://doi.org/10.5194/hess-15-1109-2011.

Kubota, T., Shige, S., Hashizurne, H., Aonashi, K., Takahashi, N., Seto, S., Hirose, M., Takayabu, Y.N., Ushio, T., Nakagawa, K., Wanami, K., Kachi, M. and Okamoto, K. (2007) Global precipitation map using satellite-bornemicrowave radiometers by the GSMaP project: production and validation. *IEEE Transactions on Geoscience and Remote Sensing*, 45, 2259–2275.

Li, Z., Yang, D. and Hong, Y. (2013) Multi-scale evaluation of high-resolution multi-sensor blended global precipitation products over the Yangtze River. *Journal of Hydrology*, 500, 157–169.

Liu, C. and Zipser, E.J. (2015) The global distribution of largest, deepest and most in- tense precipitation systems. *Geophysical Research Letters*, 42, 3591–3595. https://doi.org/10.1002/ 2015GL063776.

McCollum, J.R., Krajewski, W.F., Ferraro, R.R. and Ba, M.B. (2002) Evaluation of biases of satellite rainfall estimation algorithms over the continental United States. *Journal of Applied Meteorology*, 41, 1065–1080.

Mei, Y., Anagnostou, E.N., Nikolopoulos, E.I. and Borga, M. (2014) Error analysis of satellite precipitation products in mountainous basins. *Journal of Hydrometeorology*, 15, 1778–1793. https://doi.org/10.1175/JHM-D-13-0194.1.

Melo, D.C.D., Xavier, A.C., Bianchi, T., Oliveira, P.T.S., Scanlon, B.R., Lucas, M.C. and Wendland, E. (2015) Performance evaluation of rainfall estimates by TRMM multi-satellite precipitation analysis 3B42V6 and V7 over Brazil. *Journal of Geophysical Research: Atmospheres*, 120, 9426–9436. https://doi.org/10.1002/2015JD023797.

Michaelides, S., Levizzani, V., Anagnostou, E., Bauer, P., Kasparis, T. and Lane, J.E. (2009) Precipitation: measurement, remote sensing, climatology and modeling. *Atmospheric Research*, 94(4), 512–533.

Prakash, S., Mitra, A.K., Momin, I.M., Pai, D.S., Rajagopal, E.N. and Basu, S. (2015) Comparison of TMPA-3B42 versions 6 and 7 precipitation products with gauge-based data over India for the southwest monsoon period. *Journal of Hydrometeorology*, 16(1), 346–362.

Prakash, S., Mitra, A.K., Pai, D.S. and AghaKouchak, A. (2016) From TRMM to GPM: how well can heavy rainfall be detected from space? *Advances in Water Resources*, 88, 1–7. https://doi.org/10.1016/j.advwatres.2015.11.008.

Ren, Z.H., Zhao, P. and Zhang, Q. (2010) Quality control procedures for hourly precipitation data from automatic weather stations in China [in Chinese]. *Meteorological Monographs*, 36, 123–132.

Rhee, J., Im, J. and Carbone, G.J. (2010) Monitoring agricultural drought for arid and humid regions using multi-sensor remote sensing data. *Remote Sensing of Environment*, 114, 2875–2887.

Schneider U, Becker A, Finger P, Meyer-Christoffer A, Rudolf B, Ziese M. 2011. GPCC full data reanalysis version 6.0 at 1.0°: monthly land-surface precipitation from rain-gauges built on GTS-based and historic data, doi: https://doi.org/10.5676/DWD_GPCC/FD_M_V6_100.

Sharifi, E., Steinacker, R. and Saghafian, B. (2016) Assessment of GPM-IMERG and other precipitation products against gauge data under different topographic and climatic conditions in Iran: preliminary results. *Remote Sensing*, 8, 135. https://doi.org/10.3390/rs8020135.

Shen, Y., Xiong, A., Wang, Y. and Xie, P. (2010) Performance of high-resolution satellite precipitation products over China. *Journal of Geophysical Research*, 115, D02114. https://doi.org/10.1029/2009JD012097.

Shen, Y., Zhao, P., Pan, Y. and Yu, J. (2014) A high spatiotemporal gauge-satellite merged precipitation analysis over China. *Journal of Geophysical Research: Atmospheres*, 119, 3063–3075. https://doi.org/10.1002/2013JD020686.

Sorooshian, S., Hsu, K.L., Gao, X., Gupta, H.V., Imam, B. and Braithwaite, D. (2000) Evaluation of PERSIANN system satellite-based estimates of tropical rainfall. *Bulletin of the American Meteorological Society*, 81, 2035–2046.

Sorooshian, S., AghaKouchak, A., Arkin, P., Eylander, J., Foufoula-Georgiou, E., Harmon, R., Hendrickx, J.M.H., Imam, B., Kuligowski, R., Skahill, B. and Skofronick-Jackson, G. (2011) Advanced

concepts on remote sensing of precipitation at multiple scales. *Bulletin of the American Meteorological Society*, 92, 1353–1357.

Stampoulis, D. and Anagnostou, E.N. (2012) Evaluation of global satellite rainfall products over continental Europe. *Journal of Hydrometeorology*, 13, 588–603.

Su, F., Hong, Y. and Lettenmaier, D.P. (2008) Evaluation of TRMM multisatellite precipitation analysis (TMPA) and its utility in hydrologic prediction in the La Plata Basin. *Journal of Hydrometeorology*, 9, 622–640.

Sunilkumar, K., Rao, T.N., Saikranthi, K. and Rao, M.P. (2015) Comprehensive evaluation of multisatellite precipitation estimates over India using gridded rainfall data. *Journal of Geophysical Research: Atmospheres*, 120, 8987–9005. https://doi.org/10.1002/2015JD023437.

Tang, L., Tian, Y., Yan, F. and Habib, E. (2015) An improved procedure for the validation of satellite-based precipitation estimates. *Atmospheric Research*, 163, 61–73. https://doi.org/10.1016/j.atmosres.2014.12.016.

Tang, G., Ma, Y., Long, D., Zhong, L. and Hong, Y. (2016) Evaluation of GPM Day-1 IMERG and TMPA version-7 legacy products over mainland China at multiple spatiotemporal scales. *Journal of Hydrology*, 533, 152–167. https://doi.org/10.1016/j.jhydrol.2015.12.008.

Tian, Y. and Peters-Lidard, C.D. (2007) Systematic anomalies over inland water bodies in satellite-based precipitation estimates. *Geophysical Research Letters*, 34, L14403. https://doi.org/10.1029/2007GL030787.

Tian, Y. and Peters-Lidard, C.D. (2010) A global map of uncertainties in satellite-based precipitation measurements. *Geophysical Research Letters*, 37, L24407. https://doi.org/10.1029/2010GL046008.

Tian, Y., Peters-Lidard, C.D., Eylander, J.B., Joyce, R.J., Huffman, G.J., Adler, R.F., Hsu, K., Turk, F.J., Garcia, M. and Zeng, J. (2009) Component analysis of errors in satellite-based precipitation estimates. *Journal of Geophysical Research*, 114, D24101. https://doi.org/10.1029/2009JD011949.

TRMM Science Team. 2013. Post-real-time research-grade product of TRMM Multi-Satellite Precipitation Analysis (TMPA), 3B42 version 7. NASA Goddard Earth Science Data and Information Services Center. Available at: ftp://arthurhou.pps.eosdis.nasa.gov/trmmdata/ [Accessed January 2013].

Wang, P. and Zhu, B. (2016) Estimating the contribution of industry structure adjustment to the carbon intensity target: a case of Guangdong. *Sustainability*, 8, 355. https://doi.org/10.3390/su8040355.

Wang, D., Wang, X., Liu, L., Wang, D., Huang, H. and Pan, C. (2016) Evaluation of CMPA precipitation estimate in the evolution of typhoon-related storm rainfall in Guangdong, China. *Journal of Hydroinformatics*, 18, 1055–1068. https://doi.org/10.2166/hydro.2016.241.

Wang, D., Wang, D., Qi, X., Liu, L. and Wang, X. (2018) Use of high-resolution precipitation observations in quantifying the effect of urban extent on precipitation characteristics for different climate conditions over the Pearl River Delta, China. *Atmospheric Science Letters*, 19, 1–8. https://doi.org/10.1002/asl.820.

Xie, P. and Arkin, P.A. (1998) Global monthly precipitation estimates from satellite-observed outgoing longwave radiation. *Journal of Climate*, 11, 137–164.

Xie, P. and Xiong, A. (2011) A conceptual model for constructing high-resolution gauge–satellite merged precipitation analyses. *Journal of Geophysical Research: Atmospheres*, 116, D21106. https://doi.org/10.1029/2011jd016118.

Xu, R., Tian, F., Yang, L., Hu, H., Lu, H. and Hou, A. (2017) Ground validation of GPM IMERG and TRMM 3B42V7 rainfall products over southern Tibetan Plateau based on a high-density rain gauge network. *Journal of Geophysical Research: Atmospheres*, 122, 910–924. https://doi.org/10.1002/2016JD025418.

Xue, X., Hong, Y., Limaye, A.S., Gourley, J.J., Huffman, G.J., Khan, S.I., Dorji, C. and Chen, S. (2013) Statistical and hydrological evaluation of TRMM-based multi-satellite precipitation analysis over the Wangchu Basin of Bhutan: are the latest satellite precipitation products 3B42V7 ready for use in ungauged basins? *Journal of Hydrology*, 499, 91–99.

Yong, B., Ren, L.L., Hong, Y., Wang, J.H., Gourley, J.J., Jiang, S.H., Chen, X. and Wang, W. (2010) Hydrologic evaluation of multisatellite precipitation analysis standard precipitation products in basins beyond its inclined latitude band: a case study in Laohahe basin, China. *Water Resources Research*, 46, W07542. https://doi.org/10.1029/2009WR008965.

Yong, B., Liu, D., Gourley, J.J., Tian, Y., Huffman, G.J., Ren, L.L. and Hong, Y. (2015) Global view of real-time TRMM multi-satellite precipitation analysis: implication to its successor global precipitation measurement mission. *Bulletin of the American Meteorological Society*, 96, 283–296. https://doi.org/10.1175/BAMS-D-14-00017.1.

Zhou, T., Yu, R., Chen, H., Dai, A. and Pan, Y. (2008) Summer precipitation frequency, intensity, and diurnal cycle over China: a comparison of satellite data with rain gauge observations. *Journal of Climate*, 21, 3997–4010.

How to cite this article: Wang D, Wang X, Liu L, Wang D, Huang H, Pan C. Evaluation of TMPA 3B42V7, GPM IMERG and CMPA precipitation estimates in Guangdong Province, China. *Int J Climatol*. 2018;1–18. https://doi.org/10.1002/joc.5839